*Supplementary Information for*

# Enhanced the solar-to-hydrogen efficiency for photocatalytic water splitting based on polarized heterostructure: The role of intrinsic dipole in heterostructures

Xinyi Liu,[a] Peng Cheng, [a] Xiuhai Zhang,[b] Tao Shen,[a] Jia Liu,[a] Ji-Chang Ren,[a] Hongqiang Wang,[b]* Shuang Li[a]* and Wei Liu[a]*

[a]Nano and Heterogeneous Materials Center, School of Materials Science and Engineering, Nanjing University of Science and Technology, Nanjing 210094, China

[b]State Key Laboratory of Solidification Processing, Center for Nano Energy Materials, School of Materials Science and Engineering, Northwestern Polytechnical University and Shaanxi Joint Laboratory of Graphene, Xi'an 710072, China

*Email: lishuang@njust.edu.cn, hongqiang.wang@nwpu.edu.cn, and weiliu@njust.edu.cn

**Table S1** Calculated lattice parameters $a_0$ and total heights $h$, bond lengths, and band gap $E_g$ at the PBE level for $M_2XY$ and $E_g$ at the HSE level $M_2X_3$ monolayers. These values agree well with previous reports.[1-4]

| Materials | $a_0$(Å) | $h$(Å) | $d_{M\text{-}M}$(Å) | $d_{M\text{-}Se}$(Å) | $d_{M\text{-}S}$(Å) | $d_{M\text{-}Te}$(Å) | $E_g$ (eV ) |
|---|---|---|---|---|---|---|---|
| $In_2SSe$ | 4.00 | 5.24 | 2.77 | 2.66 | 2.58 | – | 1.61 |
| $In_2STe$ | 4.15 | 5.32 | 2.77 | – | 2.62 | 2.83 | 1.08 |
| $In_2SeTe$ | 4.21 | 5.45 | 2.77 | 2.71 | – | 2.84 | 1.19 |
| $Ga_2SSe$ | 3.72 | 4.72 | 2.46 | 2.47 | 2.39 | – | 2.08 |
| $Ga_2STe$ | 3.90 | 4.78 | 2.45 | – | 2.45 | 2.64 | 0.99 |
| $Ga_2SeTe$ | 3.98 | 4.88 | 2.45 | 2.55 | – | 2.66 | 1.29 |
| $In_2S_3$ | 3.94 | 6.44 | – | – | – | – | 1.94 |
| $In_2Se_3$ | 4.11 | 6.82 | – | – | – | – | 1.37 |
| $In_2Te_3$ | 4.41 | 7.36 | – | – | – | – | 1.12 |
| $Ga_2S_3$ | 3.65 | 5.98 | – | – | – | – | 2.56 |
| $Ga_2Se_3$ | 3.84 | 6.36 | – | – | – | – | 1.64 |
| $Ga_2Te_3$ | 4.16 | 6.93 | – | – | – | – | 0.72 |

**Fig. S1**. The partial charge analysis of the conduction band minimum (CBM) and valence band maximum (VBM) of $M_2XY$ and $M_2X_3$ monolayers.

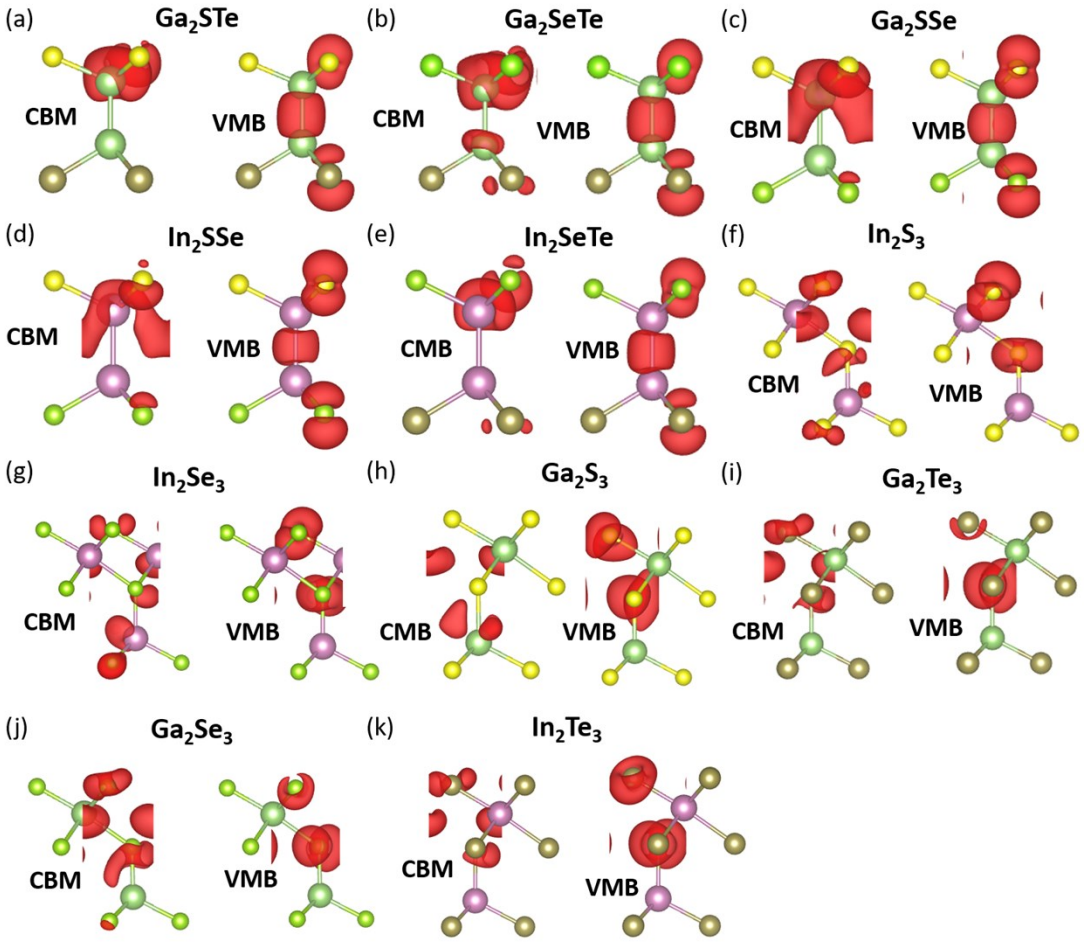

**Fig. S2.** Top and side views of configurations for vertical $M_2XY$ and $M_2X_3$ heterostructures with four possible stacking modes.

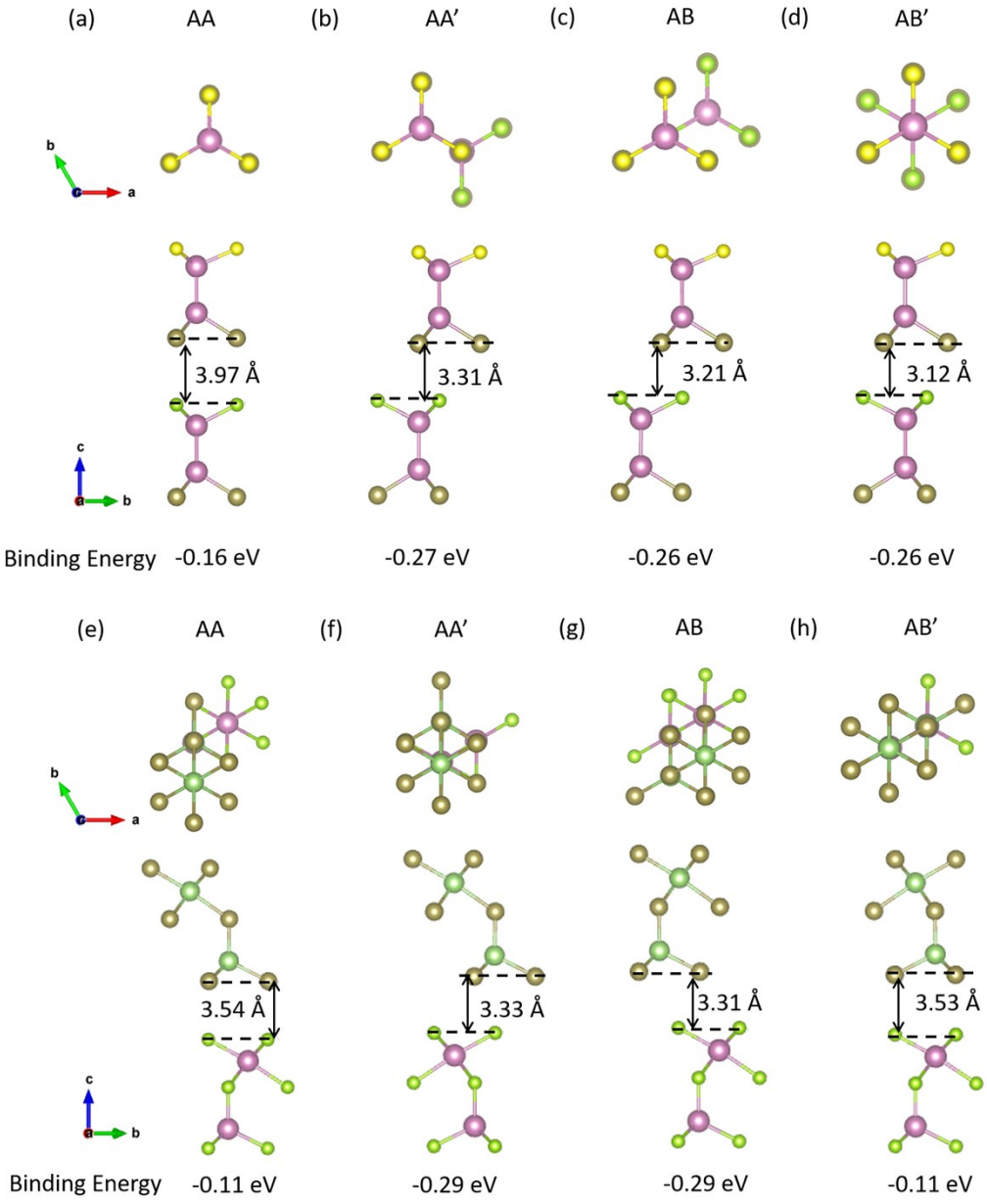

**Table S2** Interlayer distance $d_I$ and binding energy $E_b$ of vertical $M_2XY$ and $M_2X_3$ heterostructures in different types of stacking. The binding energy is calculated by the following formula: $E_b=(E_{hetero} - E_{L1} - E_{L2})$, where the $E_{hetero}$, $E_{L1}$ and $E_{L2}$ represent the total energy of heterostructures, and the individual component of single $M_2XY$ and $M_2X_3$ layers in unit cell, respectively.

| Stacking models | AA | | AA' | | AB | | AB' | |
|---|---|---|---|---|---|---|---|---|
| | $d_I$ (Å) | $E_b$ (eV) | $d_I$ (Å) | $E_b$ (eV) | $d_I$ (Å) | $E_b$ (eV) | $d_I$ (Å) | $E_b$ (eV) |
| $SIn_2Te$-$SGa_2Te$ | 3.85 | -0.17 | 3.17 | -0.25 | 3.24 | -0.24 | 3.18 | -0.25 |
| $SGa_2Te$-$SIn_2Te$ | 3.89 | -0.16 | 3.11 | -0.25 | 3.24 | -0.24 | 3.16 | -0.25 |
| $SIn_2Te$-$SeIn_2Te$ | 3.97 | -0.16 | 3.11 | -0.27 | 3.21 | -0.26 | 3.12 | -0.26 |
| $SeIn_2Te$-$SIn_2Te$ | 3.92 | -0.16 | 3.27 | -0.27 | 3.26 | -0.27 | 3.10 | -0.28 |
| $In_2Te_3$-$Ga_2Te_3$ | 3.58 | -0.12 | 3.35 | -0.29 | 3.33 | -0.28 | 3.58 | -0.13 |
| $Ga_2Te_3$-$In_2Te_3$ | 3.57 | -0.11 | 3.33 | -0.29 | 3.37 | -0.28 | 3.57 | -0.11 |
| $In_2Se_3$-$In_2Te_3$ | 3.53 | -0.10 | 3.43 | -0.28 | 3.43 | -0.28 | 3.56 | -0.11 |
| $In_2Te_3$-$In_2Se_3$ | 3.51 | -0.09 | 3.43 | -0.28 | 3.39 | -0.27 | 3.56 | -0.11 |
| $Ga_2Te_3$-$In_2Se_3$ | 3.54 | -0.11 | 3.33 | -0.29 | 3.31 | -0.29 | 3.53 | -0.11 |
| $In_2Se_3$-$Ga_2Te_3$ | 3.54 | -0.13 | 3.32 | -0.32 | 3.29 | -0.31 | 3.53 | -0.12 |

**Table S3** T The charge transfer *Q* and internal electric filed $E_{in}$ of vertical $M_2XY$ and $M_2X_3$ heterostructures in different types of stacking.

| | $SIn_2Te$-$SGa_2Te$ | $SGa_2Te$-$SIn_2Te$ | $SIn_2Te$-$SeIn_2Te$ | $SeIn_2Te$-$SIn_2Te$ | $In_2Te_3$-$Ga_2Te_3$ |
|---|---|---|---|---|---|
| Q (e) | 0.017 | 0.016 | 0.017 | 0.015 | 0.014 |
| $E_{in}$ (eV) | 0.52 | 0.32 | 0.45 | 0.36 | 0.37 |
| | $Ga_2Te_3$-$In_2Te_3$ | $In_2Se_3$-$In_2Te_3$ | $In_2Te_3$-$In_2Se_3$ | $Ga_2Te_3$-$In_2Se_3$ | $In_2Se_3$-$Ga_2Te_3$ |
| Q (e) | 0.016 | 0.012 | 0.023 | 0.025 | 0.012 |
| $E_{in}$ (eV) | 0.37 | 0.025 | 0.58 | 0.65 | 0.039 |

**Table S4** The work functions WF (eV) for up and down surfaces of $M_2XY$, $M_2X_3$ and InS monolayers.

| Surface | $In_2STe$ | $In_2SeTe$ | $Ga_2STe$ | $In_2Se_3$ | $In_2Te_3$ | $Ga_2Te_3$ | InS |
|---|---|---|---|---|---|---|---|
| up | 6.02 | 4.88 | 5.72 | 6.24 | 5.28 | 5.32 | 6.22 |
| down | 4.64 | 4.46 | 4.96 | 5.02 | 4.22 | 4.43 | 6.22 |

**Fig. S3.** The band alignments of the type-II junction mode for heterostructures $SIn_2Te$-$SeIn_2Te$ (a) and $In_2Se_3$-$Ga_2Te_3$ (b), respectively. The black arrows represent the charge transfer and e–h recombination process. The plane-average charge density difference $\Delta\rho$ for heterostructures $SIn_2Te$-$SeIn_2Te$ (c) and $In_2Se_3$-$Ga_2Te_3$ (d). The positive and negative value in $\Delta\rho$ indicate electron accumulation and depletion, respectively. The red (green) colour corresponds to the charge accumulation (depletion). The $E_{in}$ represents the built-in electric field at the interface of heterostructures.

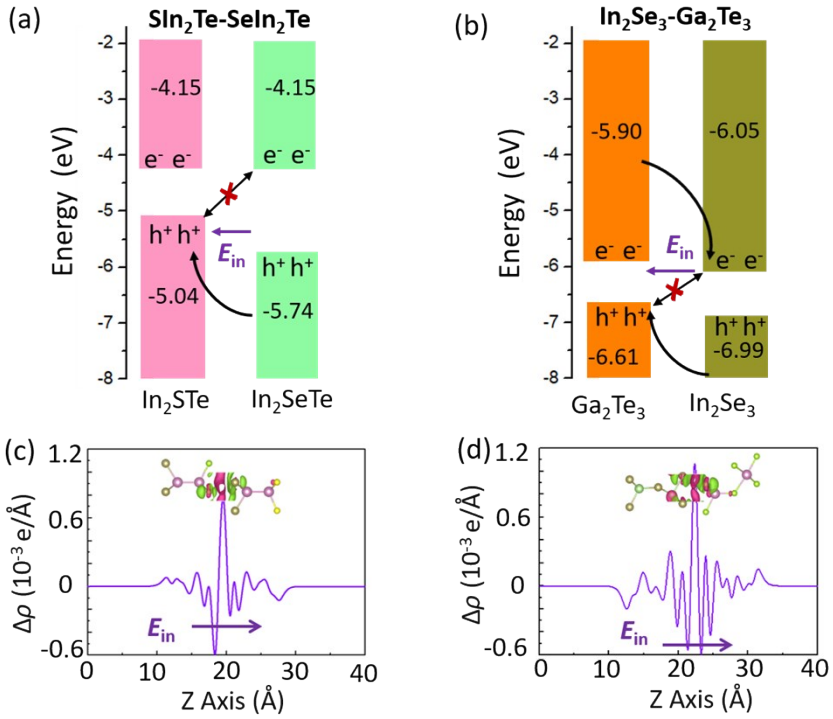

**Fig. S4.** (a) Plane-average charge density difference $\Delta\rho$ of $In_2Se_3/SnP_3$ heterostructure. The positive and negative value in $\Delta\rho$ indicate electron accumulation and depletion, respectively. The red (green) colour corresponds to the charge accumulation (depletion). (b) The schematic plot of vacuum level for $In_2Se_3/SnP_3$ heterostructure. It is noted that there is a big difference $\Delta\Phi$ for the vacuum level between the $SnP_3$ surface and $In_2Se_3$ surface (larger than the intrinsic $\Delta\Phi$ for $In_2Se_3$ layer), which means that there is an internal electric field pointing to $In_2Se_3$ layer from $SnP_3$ layer at the interface of the heterostructure.